Near-Infrared Extinction and Molecular Cloud Structure

Charles J. Lada
Harvard-Smithsonian Center for Astrophysics

João F. Alves and Marco Lombardi
European Southern Observatory

A little more than a decade has passed since the advent of large-format infrared array cameras opened a new window on molecular cloud research. This powerful observational tool has enabled dust extinction and column density maps of molecular clouds to be constructed with unprecedented precision, depth, and angular resolution. Near-infrared extinction studies can achieve column density dynamic ranges of $0.3 < A_V < 40$ mag ($6 \times 10^{20} < N < 10^{23}$ cm^{-2}), allowing with one simple tracer a nearly complete description of the density structure of a cloud free from the uncertainties that typically plague measurements derived from radio spectroscopy and dust emission. This has led in recent years to an empirical characterization of the evolutionary status of dense cores based on the shapes of their radial column density profiles and revealed the best examples in nature of Bonnor-Ebert spheres. Widefield infrared extinction mapping of large cloud complexes provides the most complete inventory of cloudy material that can be derived from observations. Such studies enable the measurement of the mass function of dense cores within a cloud, a critical piece of information for developing an understanding of the origin of the stellar IMF. Comparison with radio spectroscopic data has allowed detailed chemical structure studies of starless cores and provided some of the clearest evidence for differential depletion of molecular species in cold gaseous configurations. Recent studies have demonstrated the feasibility of infrared extinction mapping of galactic molecular clouds (GMCs) in external galaxies, enabling the fundamental measurement of the GMC mass function in these systems. In this contribution we review recent results arising from this powerful technique, ranging from studies of Bok globules to local GMCs, to GMCs in external galaxies.

1. INTRODUCTION

Although first discovered in the late eighteenth century with visual telescopic observations by William and Caroline Herschel (*Herschel,* 1785), well over a century passed before photographic observations of *Barnard* (1919) and *Wolf* (1923) established dark nebulae as discrete, optically opaque interstellar clouds. Wolf's photographic photometry further demonstrated that the opaque material in these clouds consisted of solid, small particles now known as interstellar dust grains. For nearly three decades astronomers could not discern whether such nebulae contained gaseous matter or were solely made up of dust. Indeed, in the 1950s the discovery of the 21-cm line of H I led to the measurement of a general correlation between dust absorption and H I emission at low extinctions (*Lilley,* 1955). However, the first searches for H I gas toward the centers of dark nebulae found H I emission to be either weak or entirely absent (*Bok et al.,* 1955; *Heiles,* 1969). This fact led *Bok et al.* (1955) to the prescient suggestion that if any gas existed within these nebulae, it had to be molecular in form.

The discovery of a cold molecular component of the interstellar medium primarily via CO observations in the early 1970s (e.g., *Wilson et al.,* 1970) quickly lead to the realization that dark clouds were molecular clouds, consisting almost entirely of molecular hydrogen mixed with small amounts of interstellar dust and trace amounts of more complex molecular species. Over the last 30 years infrared observations from space and the ground (e.g., *Becklin and Neugebauer,* 1967; *Strom et al.,* 1975; *Wilking et al.,* 1989; *Yun and Clemens,* 1990; *Lada,* 1992) have established the true astrophysical importance of molecular clouds as the sites of all star formation in the Milky Way.

Knowledge of the structure and physical conditions in molecular clouds is of critical importance for understanding the process of star formation. Such observations can set the initial conditions for star formation and enable the direct investigation of the evolution of cloudy material as it is transformed into stellar form. However, although almost entirely composed of molecular hydrogen, two factors render H_2 generally unobservable in molecular clouds. First, because it is a homonuclear molecule, it lacks a permanent dipole moment and its rotational transitions are extremely weak. Second, being the lightest molecule, its lowest energy rotational transitions are at mid-infrared wavelengths, which are simultaneously inaccessible to observation from Earth and too energetic to be collisionally excited at the cold temperatures (e.g., 10 K) that are characteristic of dark

molecular clouds. Thus the structure and physical conditions of dark clouds must be derived from H_2 surrogates, namely dust and trace molecular gases such as CO, NH_3, and HCN.

Despite early promise, use of molecular lines from trace molecular species for this purpose has turned out to be severely hampered by the presence of significant variations in opacities, chemical abundances, and excitation conditions within dark nebulae. Yet most of what we know of the physical conditions in molecular clouds derives from such studies. Observations of dust may be the most direct and reliable way to trace the hydrogen content of a molecular cloud. This is because of the constancy of the gas-to-dust ratio in interstellar clouds, which is observationally well established (e.g., *Lilley,* 1955; *Ryter et al.,* 1975; *Bohlin et al.,* 1978; *Predehl and Schmitt,* 1995). In principle, the dust content of a cloud can be traced through measurements of either dust emission or extinction (i.e., absorption plus scattering of background starlight). Interpretation of measurements of dust emission is complicated by the fact that the observed emission is a product of dust column density and dust temperature. For the range of temperatures characteristic of dark clouds (8–50 K), dust emission is brightest and most readily detected at far-infrared wavelengths. This emission is near the peak and often on the Wien side of the corresponding Planck curve and thus nonlinearly sensitive to the temperature of dust along the line-of-sight. Moreover, because of the opacity of our atmosphere at these wavelengths such observations are best carried out on space platforms. On the other hand, *dust extinction* is independent of *dust temperature,* and measurements of dust extinction are directly proportional to dust optical depth and column density and thus measurement of dust extinction is the most direct and straightforward way to detect and map the dust content of a cloud. There are two observational techniques used to make such extinction measurements: the classical method of star counts (e.g., *Bok,* 1956) and the method of measuring stellar color excess (e.g., *Lada et al.,* 1994).

2. MEASURING DUST EXTINCTION

2.1. Star Counts

Throughout the last century the general method to derive and map the extinction through a dark cloud has been the use of optical star counts (e.g., *Wolf,* 1923; *Bok,* 1956; *Dickman,* 1978; *Cernicharo and Bachiller,* 1984). In this method typically a rectilinear grid is overlaid on an image of the target cloud, and the number of stars to a fixed limiting magnitude is counted in each box of the grid. These counts are compared to those in a nearby, unobscured region. The extinction is then given by

$$A_\lambda = \log(N_{off}/N_{on})/b_\lambda \quad (1)$$

Here N is the surface density of stars either on or off the cloud and b is the slope of the logarithmic cumulative luminosity function of stars in the control field. One of the most impressive studies of this type is the recent work of *Dobashi et al.* (2005). They used the Digitized Sky Survey to obtain star counts and a map of extinction encompassing the entire galactic plane. In the process they were able to identify 2448 dark clouds. However, such measurements suffer from a number of limitations, the most significant of which is the uncertainty due to Poisson statistics. For example, at optical wavelengths (using the POSS) it takes only about 4–5 mag of visual extinction to reduce the number of stars in a single counting pixel to unity in a typical arcminute-sized region of the galactic plane. Somewhat higher values of extinction (A_V ~ 5–9 mag) can be measured, but at the significant expense of angular resolution and thus the loss of structural information (*Cambresy,* 1999). For example, the widefield maps of *Dobashi et al.* (2005) were limited to resolutions of 6 and 18 arcminutes. One can take advantage of the extinction law and instead perform star counts at near-infrared wavelengths where extinction is significantly reduced compared to the optical regime. Therefore, significantly larger numbers of background stars can be observed through a dark cloud in the infrared than at traditional optical wavelengths. Such measurements can attain higher values (10–20 mag) of visual extinction without sacrificing too much angular resolution (e.g., *Lada et al.,* 1994; *Harvey et al.,* 2001, 2003; *Pagani et al.,* 2004; *Kandori et al.,* 2005). However, multiwavelength infrared observations can produce even deeper and much more direct extinction determinations with greatly improved angular resolution and smaller overall uncertainties by using measurements of near-infrared color-excess to derive the extinction. With large-format infrared arrays it is now possible to use moderate-sized telescopes to detect and simultaneously determine the colors of thousands of stars behind a dark molecular cloud.

2.2. Near-Infrared Color Excess: NICE and NICER

Because of the wavelength dependence of extinction (see Fig. 1) it is advantageous to observe at the longest wavelength possible to penetrate the most heavily obscured regions of a dark cloud. The opacity of Earth's atmosphere severely limits observations at wavelengths much longer than 2 μm. The standard near-infrared H (1.65 μm) and K (2.2 μm) bands are closely matched to windows of atmospheric transmission and represent the longest wavelengths for optimized groundbased observation with infrared array cameras. Moreover, typical field stars are relatively bright in the near-infrared since these wavelengths are near the peak of their stellar energy distributions, and thus these stars are readily detected with existing infrared cameras on modest-sized telescopes. Because of the wavelength dependence of extinction, light from a star suffers a change in color as well as a general diminution. The change in a star's color is much more easily measured than the change in a star's brightness. This is because the intrinsic variation in unextincted stellar colors is considerably smaller than the magnitude of the change in stellar colors induced by extinction,

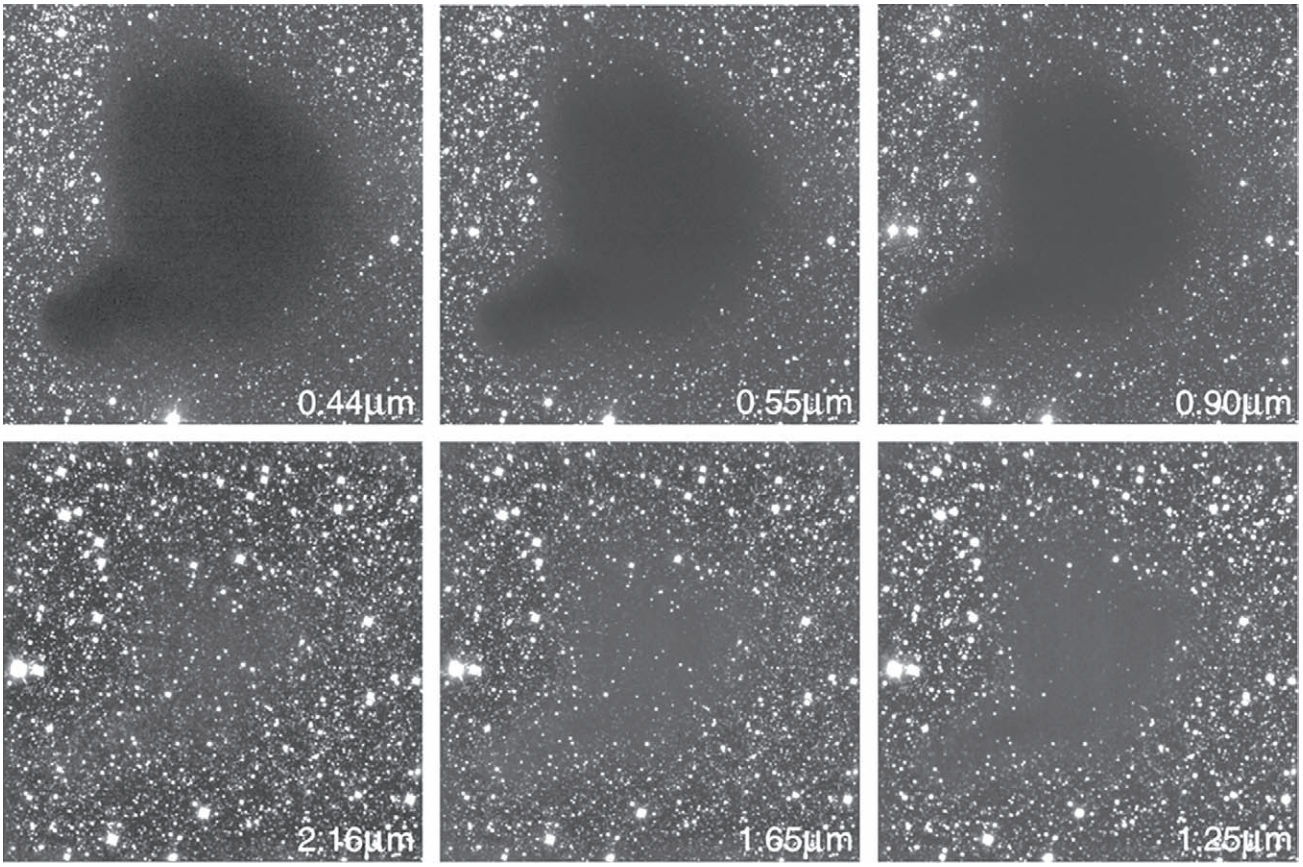

Fig. 1. Optical (BVI) and infrared (JHKs) images of the globule Barnard 68 obtained with ESO's VLT and NTT (*Alves et al.,* 2001a). This sequence shows the increasing transparency of interstellar dust with increasing wavelength. At the optical bands B (0.44 μm) and V (0.55 μm) the globule is completely opaque, while in the infrared K_s (2.16 μm) band it is almost completely transparent.

while the intrinsic variation in unextincted stellar brightnesses of background stars is comparable to and often significantly exceeds the magnitude of the diminution in stellar brightnesses caused by extinction.

The line-of-sight extinction to an individual star can be directly determined from knowledge of its color excess and the extinction law. The color excess, E(H–K), can be directly derived from observations provided the intrinsic color of the star is known

$$E(H–K) = (H–K)_{observed} – (H–K)_{intrinsic} \quad (2)$$

The intrinsic (H–K) colors of normal main-sequence and giant stars are small and span a narrow range in magnitude (0.0–0.3 mag for stars with spectral types between A0 and late M).

One expects the range in intrinsic colors of background field stars to span an even smaller range since such stars span a relatively narrow range in spectral type (typically K and M). Observations of field stars in nearby (unobscured) control regions off the target cloud can be used very effectively to determine the intrinsic colors of background stars provided that the control field stars themselves do not suffer significant additional extinction in comparison to the stars in the target field (e.g., from unrelated background clouds along the same line-of-sight).

With the assumption that all the background field stars observed through a target molecular cloud are identical in nature to those in the control field, we can use the mean H–K color of the control field stars to approximate the intrinsic H–K color of all stars background to the cloud

$$(H–K)_{intrinsic} \equiv <(H–K)>_{control} \quad (3)$$

The infrared color excess is directly related to the extinction (at any wavelength) via the extinction law

$$A_\lambda = r_\lambda^{H,K} E(H–K) \quad (4)$$

where $r_\lambda^{H,K}$ is the appropriate constant of proportionality given by the adopted extinction law (e.g., *Rieke and Lebosky,* 1985). Use of infrared colors to measure extinction is known as the Near-Infrared Color Excess (NICE) method of extinction determination.

As shown by *Lombardi and Alves* (2001), one can take full advantage of observations carried out in multiple (>2) bands to obtain even more accurate column density measurements. The improved technique, called NICER (NICE

Revisited), optimally balances the information from different bands and different stars. As a byproduct of the analysis, NICER also allows one to evaluate the expected error on the column density map, which is useful to estimate the significance for the detection of substructures and cores. The NICER technique is better described by noting that, in principle, equations (2) and (4) can be equally well applied to any combination of infrared bands (e.g., the color H–K usually used in NICE, or the alternative JH color, if the J-band photometry is available): Hence, this way we can have several different estimates of the cloud column density. The NICER technique finds an optimal linear combination of the column density estimates from the different bands. For example, in the case of three bands J, H, and K, the extinction is estimated as

$$A_\lambda = b_\lambda^{H,K} E(H–K) + b_\lambda^{J,H} E(J–H) \qquad (5)$$

and the coefficients $b_\lambda^{H,K}$ and $b_\lambda^{J,H}$ are found by requiring that (1) the column density estimate is unbiased and (2) it has minimum variance. The first condition, by inspection of equation (4), implies $b_\lambda^{H,K} r_\lambda^{H,K} + b_\lambda^{J,H} r_\lambda^{J,H} = 1$, while the second depends on the intrinsic scatter in the infrared colors and on the individual errors on the photometric measurements of each star (see *Lombardi and Alves,* 2001, for details). When applied to typical NIR observations, the NICER method is able to reduce by a factor of 2 the average variance of the NICE column density measurements, thus improving the maximum resolution achievable. More significantly, use of NICER greatly improves the overall sensitivity of the extinction measurements at low extinctions ($0.5 < A_V < 2.0$ mag). Its implementation thus enables the mapping of the outer envelopes of molecular clouds, regions that cannot be traced by CO observations because of the dissociation of CO by the interstellar radiation field.

A further enhancement on the accuracy of column density measurements can be gained by using a maximum likelihood (ML) technique (*Lombardi,* 2005). The method takes advantage of both the multicolor distribution of reddened stars and of their spatial distribution. In other words, the ML method optimally integrates the color excess and star counts methods. The ML technique is especially convenient in the high-density cores of molecular clouds, and in the presence of contamination by foreground stars.

Although the exact number of background stars that can be detected behind a molecular cloud depends on its galactic latitude and longitude, its angular size, and the sensitivity of the observations, a modest depth (i.e., $K \leq 16$) infrared imaging survey can easily yield colors for thousands of background stars behind a typical nearby dark cloud. The resulting database of infrared color excesses and source positions would represent a map of the distribution of color excess (and extinction) through the cloud obtained with extraordinarily high (pencil-beam) angular resolution. However, we can expect this map to be randomly and heavily undersampled in space because of various observational selection effects expected in a magnitude-limited survey (e.g., the observed surface density of background stars is a function of detector sensitivity, galactic longitude and latitude, and extinction). The data in such a survey can also be used to construct an ordered and uniformly sampled map of the distribution of color excess through the cloud by smoothing the angular resolution of the observations. The smoothing functions or kernels that have been employed are typically of fixed angular resolution and either in the shape of a square (e.g., *Lada et al.,* 1994) or a two-dimensional gaussian [better for comparison with radio data (e.g., *Alves et al.,* 1999, 2001a)]. Cambresy and co-workers have advocated the use of an adaptive smoothing kernel that constantly adjusts the size of the kernel to maintain a constant number of stars and a constant noise level in each pixel of a map (*Cambresy et al.,* 1997, 2002; *Cambresy,* 1999). This method produces lower angular resolution at the highest extinctions, but eliminates empty pixels or pixels with only a single star that might otherwise occur in maps with fixed angular resolution.

3. EXTINCTION MAPPING OF CLOUD CORES

Low-mass dense cores within large molecular complexes and isolated dense cores (also known as Bok globules) are the simplest configurations of dense molecular gas and dust known to form stars (e.g., *Benson and Myers,* 1989; *Yun and Clemens,* 1990). They have been long recognized as important laboratories for investigating the physical processes that lead to the formation of stars and planets (e.g., *Bok,* 1948). These cores come in two varieties: protostellar and starless. Detailed knowledge of the structure of both types of cores is essential for obtaining an empirical picture of the evolution of dense gas to form stars. Such information can provide critical constraints for developing an overall theory of star formation. Early work by *Tomita et al.* (1979) attempted to probe the structure of dark globules using extinction measurements derived from optical star counts of the Palomar Sky Survey. They found core structure to be characterized by very steep density gradients with power-law exponents ranging between –3 to –5. However, the high extinctions that characterized the globules limited their measurements to only the very outer regions or atmospheres of these objects and were not useful for constraining the overall structure of these cores.

It has been long understood that infrared observations could probe much larger extinctions in such objects and initial studies of globules using single-channel infrared detectors showed much promise for probing higher extinctions and obtaining more complete measurements of the structure of globules and dense cores (*Jones et al.,* 1980; *Casali,* 1986). But these studies were very limited by sensitivity and the small numbers of background stars that could be measured in the regions. The development of sensitive infrared imaging array detectors radically altered this situation. Such arrays enabled the detection of thousands of background stars behind clouds and resulted in the first detailed extinc-

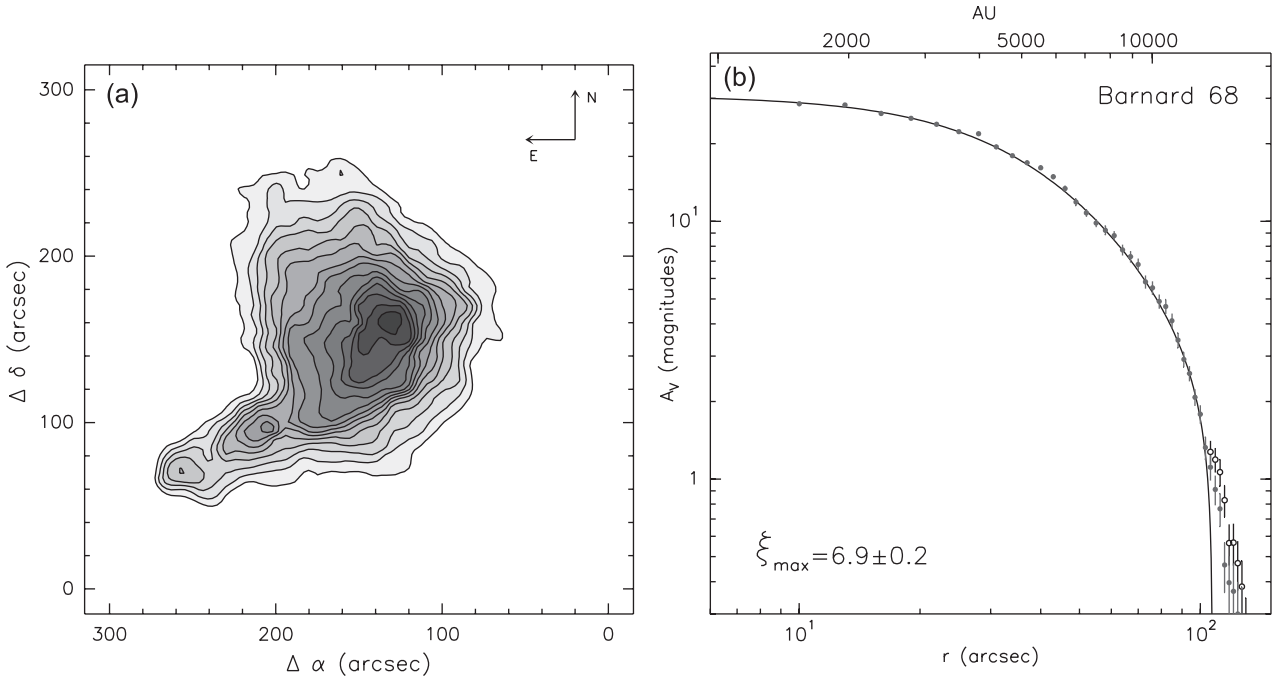

Fig. 2. **(a)** Distribution of extinction (dust column density) for the B68 cloud (see Fig. 1) derived from deep near-infrared extinction measurements sampled with a gaussian spatial filter of 10 arcsec (1000 AU) width (FWHP). **(b)** Azimuthally averaged dust column density profile for the cloud constructed with a spatial resolution of 5 arcsec (500 AU). With this resolution the radial structure of the cloud is extremely well resolved. (Open circles include the contribution of the tongue or protrusion of material at the southeast edge of the cloud; filled circles exclude this material.) Plotted for comparison is the corresponding best-fit column density profile (solid line) for a pressure-truncated, isothermal sphere (Bonnor-Ebert sphere).

tion maps of dark nebulae with high angular resolution and sufficient depth to probe the structure at relatively high extinction (*Lada et al.,* 1994, 1999; *Alves et al.,* 1998). Indeed, coupled with larger-aperture telescopes, such arrays also allowed deep imaging of nearby dark clouds and the ability to measure extinctions in regions of very high opacity, that is, $20 < A_V < 35$ mag (*Alves et al.,* 2001a). This is the level of extinction produced by the dense cores of dark clouds, the very places in which star formation takes place.

3.1. Starless Cores

Two of the least-understood aspects of the star-formation process are the initial conditions that describe dense cores that ultimately form stars and the origin of such dense cores from more diffuse atomic and molecular material. Deep infrared observations of starless cores or globules offer among the best opportunities to quantitatively investigate these issues. The first starless globule or core to be mapped at high resolution in dust extinction was the prominent globule Barnard 68 (B68) (*Alves et al.,* 2001a). Optical and infrared images of this globule are shown in Fig. 1. This globule is situated in front of the rich star field of the galactic bulge where the homogeneous nature of the background stars resulted in a very accurate determination of their intrinsic colors and very accurate measurements of extinction. Moreover, the high density of background stars enabled the cloud to be mapped with relatively high angular resolution.

Figure 2 shows the resulting extinction map of B68 smoothed with a 10-arcsec (~1000 AU) gaussian spatial filter. Also plotted is the radial column density profile constructed by azimuthally averaging the data into annuli of 5-arcsec (500 AU)-wide bins. The radial column density profile of this cloud is very well resolved by the observations. *Alves et al.* (2001a) showed that this profile could be extremely well fit by the predicted profile of a Bonnor-Ebert (BE) sphere.

A BE sphere is a pressure-truncated isothermal ball of gas within which internal pressure everywhere precisely balances the inward push of self-gravity and external surface pressure. The fluid equation that describes such a self-gravitating, isothermal sphere in hydrostatic equilibrium is the following well-known variant of the Lane-Emden equation

$$\frac{1}{\xi^2}\frac{d}{d\xi}\left(\xi^2\frac{d\psi}{d\xi}\right) = e^{-\psi} \qquad (6)$$

where ξ is the dimensionless radius

$$\xi = r/r_c \quad (7)$$

and r_c is the characteristic or scale radius

$$r_c = c_s/(4\pi G\rho_0)^{1/2} \quad (8)$$

where c_s is the sound speed in the cloud and ρ_0 is the density at the origin. Equation (6) is Poisson's equation in dimensionless form where $\psi(\xi)$ is the dimensionless potential and is set by the requirement of hydrostatic equilibrium to be $\psi(\xi) = -\ln(\rho/\rho_0)$. The equation can be solved using the boundary conditions that the function ψ and its first derivative are zero at the origin. Equation (6) has an infinite family of solutions that are characterized by a single parameter, the dimensionless radius at outer edge (R) of the sphere

$$\xi_{max} = R/r_c \quad (9)$$

Each solution thus corresponds to a truncation of the infinite isothermal sphere at a different outer radius, R. The external pressure at a given R must then be equal to that which would be produced by the weight of material that otherwise would extend from R to infinity in an infinite isothermal sphere. The shape of the BE density profile for a pressure-truncated isothermal cloud therefore depends on the single parameter ξ_{max}. As it turns out, the higher the value of ξ_{max}, the more centrally concentrated the cloud is. The stability of such pressure truncated clouds was investigated by *Bonnor* (1956) and *Ebert* (1955), who showed that when $\xi_{max} > 6.5$ the clouds are in a state of unstable equilibrium, susceptible to gravitational collapse.

For B68, *Alves et al.* (2001a) found the radial density profile to be extremely well fit by a Bonnor-Ebert model with $\xi_{max} = 6.9$ very close to the critically stable value. The close correspondence of the data with the BE prediction strongly suggests that this globule is a relatively stable configuration of gas in which thermal pressure is a significant source of support against gravity. This close agreement of theory and observation has very important implications for the physical and evolutionary nature of this source since it implies that the globule is a coherent dynamical unit and not a transient structure.

The nature of B68 as a thermally dominated, quasistable cloud has been decisively confirmed by molecular-line observations of *Hotzel et al.* (2002) and *Lada et al.* (2003), who found the molecular-line profiles to be characterized by thermal line widths. Indeed, the latter study showed the thermal pressure to be a factor of 5 greater than the nonthermal or turbulent pressure in the center of the cloud. Moreover, these observations demonstrated that the cloud is undergoing global oscillation around a state of overall dynamical equilibrium. In a more recent survey of globules, *Kandori et al.* (2005) found that most of the starless globules they studied are dominated by thermal pressure, similar to B68. *Tafalla et al.* (2004) also reported thermally dominated, quasistable states for two more massive cores in the Taurus dark cloud complex. These findings are in clear contradiction to and rule out the suggestion of *Ballesteros-Paredes et al.* (2003), who posited B68 (and similar cores) to be a transient dynamical fluctuation in a turbulent velocity field.

Equations (8) and (9) coupled with the extinction measurements enable the fundamental physical conditions of the globule, i.e., its temperature, central density, external pressure, size, etc., to be exquisitely specified. Indeed, if the temperature of the cloud can be independently determined from molecular line observations (e.g., NH_3), then the terms in equations (8) and (9) are overspecified and "reverse engineering" is possible, resulting in precise determination of either the cloud distance or its gas-to-dust ratio (*Alves et al.,* 2001b; *Hotzel et al.,* 2002; *Lai et al.,* 2003). Integration of the extinction map (i.e., Fig. 2) also produces a very precise estimate of the total dust mass of the cloud. With the assumption of distance and gas-to-dust ratio, a relatively accurate determination of the total cloud mass can be made with an uncertainty completely dominated by the uncertainties in these two assumed parameters.

Infrared extinction maps of a number of starless globules and cores have now been published and the cores are typically found to exhibit Bonnor-Ebert column density profiles with shapes close to the critical stability limit, similar to B68 (*Lada et al.,* 2004; *Teixeira et al.,* 2005; *Kandori et al.,* 2005). Figure 3 shows the distribution of the fit parameter ξ_{max} for a sample of mostly starless globules studied by *Kandori et al.* (2005). The concentration near the critical value is evident. Similar findings have resulted from surveys and mapping of dust continuum emission from starless cores (e.g., *Kirk et al.,* 2005). Such gaseous configurations likely represent the initial conditions for star formation in dense cores.

3.2. Protostellar Cores

Infrared extinction studies have also been carried out toward a few star-forming, protostellar cores (e.g., *Harvey et al.,* 2001; *Teixeira et al.,* 2005; *Kandori et al.,* 2005). These studies show that cores containing protostars tend to have much steeper radial column and volume density profiles than starless cores. Indeed, the central extinctions rise to such high values ($A_V > 40$ mag) in these cores that even the deepest ground- and spacebased imaging cannot detect background stars in their innermost regions. Surprisingly perhaps, the radial density profiles, where measured, can still be fit by Bonnor-Ebert curves, but these are characterized by large values of ξ_{max} (12–25) consistent with large center-to-edge density contrasts and indicative of highly unstable equilibrium configurations (see Fig. 3).

It therefore has been suggested that in the process of forming a star the shape of a core's radial density profile evolves from a relatively flat, equilibrium structure to a highly condensed collapsing structure in a systematic manner that can be quantified using a Bonnor-Ebert analysis (e.g., *Lada et al.,* 2004; *Teixeira et al.,* 2005; *Kandori et al.,* 2005). A quasistable globule or core could become unstable by either an increase in the external pressure (an external

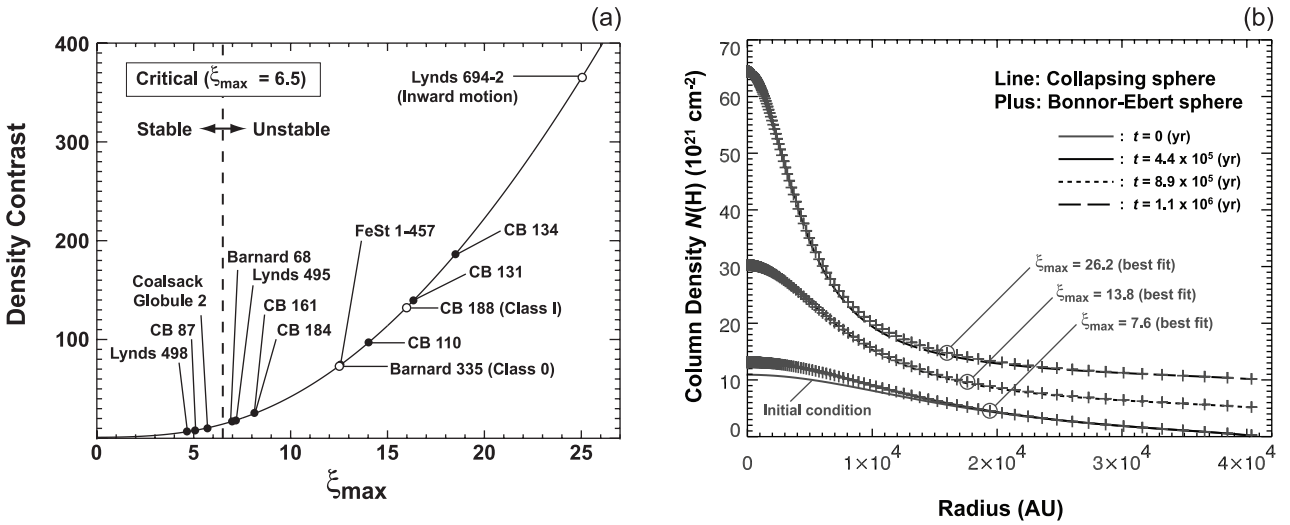

Fig. 3. **(a)** The relation of ξ_{max} to a cloud's center-to-edge density contrast for Bonnor-Ebert configurations. The distributions of the values of ξ_{max} derived from extinction observations of starless (closed symbols) and protostellar (open symbols) cores are also plotted (*Kandori et al.,* 2005). **(b)** The predicted radial column density profiles for a collapsing spherical cloud at different times (solid lines) starting from an initial state characterized by a critically stable Bonnor-Ebert sphere. The fitted Bonnor-Ebert relations are plotted as plus signs and the corresponding values of ξ_{max} are indicated. From *Kandori et al.* (2005).

perturbation) or a decrease in the internal pressure. Passage of external shocks, such as produced by supernovae or in cloud-cloud collisions, could result in abrupt increases in external pressure. Although many of these globules and cores are thermally dominated, residual magnetic fields and/or turbulence could provide significant sources of internal pressure. The dissipation of even small amounts of residual internal turbulence (*Nakano,* 1998) or ambipolar diffusion (*Shu et al.,* 1987; *Mouschovias and Ciolek,* 1998) could result in a decrease of internal pressure and instability. Recently *Kandori et al.* (2005) and *Myers* (2005) have calculated the evolution of a spherical cloud assuming that the initial condition is that of a critically stable Bonnor-Ebert configuration. These calculations demonstrate that as the cloud collapses its radial density profile maintains the shape of a Bonnor-Ebert profile with the density contrast (i.e., ξ_{max}) systematically increasing as the collapse proceeds. This effect is nicely illustrated in Fig. 3, which shows the theoretical prediction for the structure of a collapsing core at four different times (*Kandori et al.,* 2005). Also plotted are the best fit Bonnor-Ebert relations, which suggest that the evolutionary status of a collapsing core can be estimated from the instantaneous shape (parameterized by ξ_{max}) of its column density profile. Thus, *even when a dense core is out of equilibrium and collapsing,* its density structure maintains a Bonnor-Ebert like configuration, provided the initial condition was given by a critically stable Bonnor-Ebert state. Moreover, the calculations of Kandori et al. predict that the frequency distribution of ξ_{max} derived from observations should peak near the critically stable value since the timescale for evolution decreases with increasing density. This is in fact evident in the data (Fig. 3). Indeed, according to the calculations more than 60% of the total collapse time passes before the center-to-edge density contrast increases by as much as a factor of 4 over the initial critical state (*Kandori et al.,* 2005). Finally, the fact that the structure of both stable and collapsing cores can be fit by Bonnor-Ebert models indicates that the initial conditions for core collapse and star formation must be similar to those described by a critically stable Bonnor-Ebert configuration, such as B68.

The observations and calculations described above demonstrate that extinction measurements of cores and globules can be a powerful tool for constructing a quantitative empirical description of their structural evolution to form stars. As a result a more complete theoretical understanding of this process may now be closer to realization. The Bonnor-Ebert formalism appears to provide an initial theoretical framework that can describe quite well the physical process of core evolution to form stars. However, this framework will need to be refined to account for more realistic cloud geometries (e.g., *Myers,* 2005) and equations of state (e.g., *McKee,* 1999; *McKee and Holliman,* 1999). Moreover, extinction properties of a larger sample of cores and globules as well as improved characterizations of their dynamical states from molecular-line observations are clearly warranted.

4. EXTINCTION MAPPING OF CLOUD COMPLEXES

Infrared extinction mapping has also provided new information about the larger-scale structure of nearby molecular cloud complexes within which dense cores are usually embedded. Initial studies focused on nearby filamentary

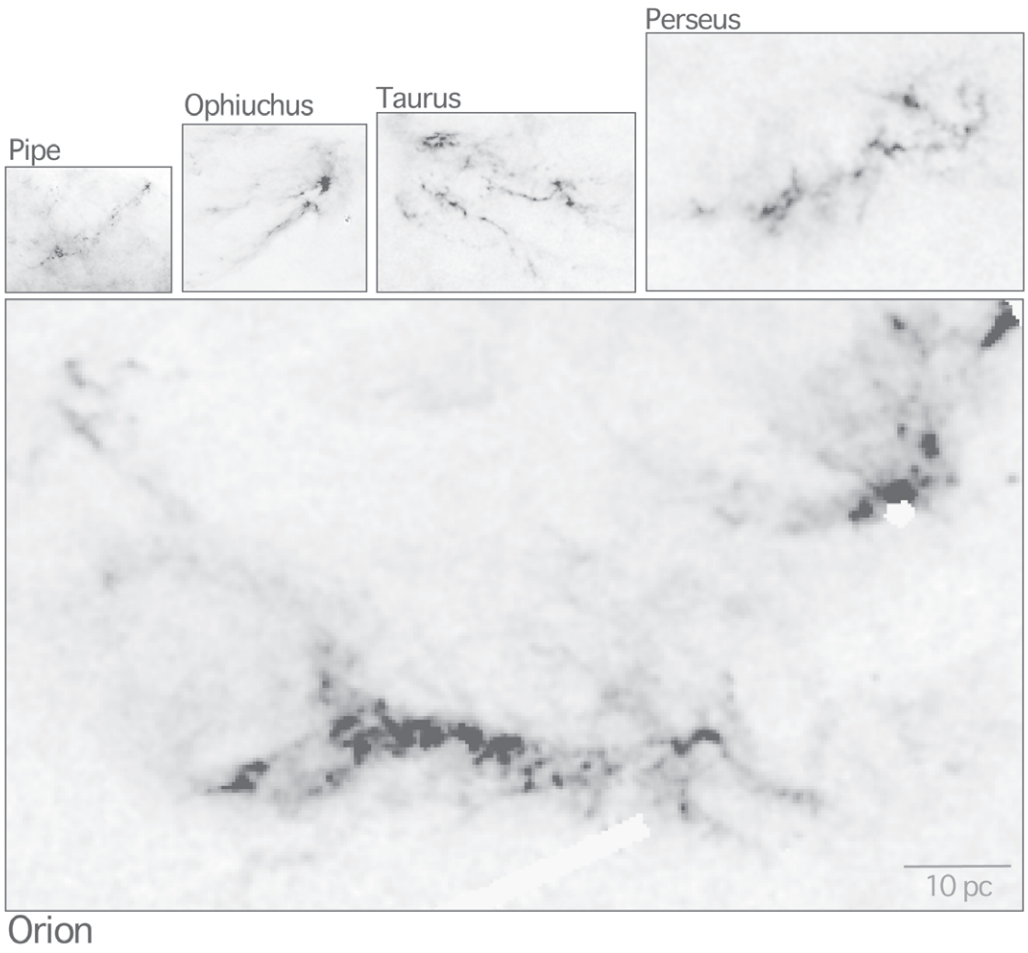

Fig. 4. NICER extinction maps of local molecular cloud complexes. The maps are shown on the same physical scale but are characterized by different angular resolutions.

clouds including IC 5146 (B168) (*Lada et al.,* 1994, 1999) and L 977 (*Alves et al.,* 1998, 1999). These studies showed that the filamentary structures exhibited smooth radial density gradients orthogonal to their main axis that are well modeled by pressure-truncated isothermal cylinders (Huard et al., in preparation). The extinction observations produced detailed measurements of the frequency distribution of extinction (i.e., the cloud mass distribution function), showing that most of the mass of a cloud is at low extinction. Only about 25–30% of the material in these dark clouds is characterized by extinctions in excess of 10 visual magnitudes (*Alves et al.,* 1999). The form of the cloud mass distribution function was also found to be consistent with that predicted in simulations of turbulent clouds (*Ostriker et al.,* 2001). Moreover, integration of such maps yields very precise estimates (to a few percent) of the masses of these clouds. However, the accuracy of such mass determinations is entirely dominated and limited by the uncertainty in the assumed distance determinations.

The availability of the 2MASS near-infrared all sky survey has enabled the construction of widefield extinction maps that can encompass the entire extent of a galactic molecular cloud (GMC) (e.g., *Cambresy et al.,* 2002; *Lombardi and Alves,* 2001). Using NICER, complete maps of a number of prominent local cloud complexes have been made. These maps are sufficiently sensitive to trace relatively low levels of extinction ($A_V \sim 0.5$ mag) and have extended the boundaries of the clouds beyond the level that can be traced by CO emission. Figure 4 shows NICER extinction maps of five prominent cloud complexes drawn to the same physical scale (*Lombardi and Alves,* 2001; *Lombardi et al.,* 2006; Lombardi and Alves, in preparation). These maps can reveal interesting structural information about the cloudy material. For example, the cumulative frequency distribution of extinction for the Pipe Nebula (*Lombardi et al.,* 2006) shows the cloud to contain only about 1% of its mass at extinctions in excess of $A_V > 10$ mag. In this respect the Pipe cloud differs from the IC 5146 and L 977 clouds having a considerably smaller fraction of its mass at these levels of extinction that are typically characteristic of star-forming material (e.g., *Johnstone et al.,* 2004). The Pipe cloud also contains much lower levels of star-formation

activity than clouds like Ophiuchus, Orion, and Taurus and may be at a much earlier stage of overall development. Further examination of its cumulative extinction distribution shows that about 30% of the cloud's mass exists at extinctions (A_V) < 2 mag, the threshold for the CO dissociation. This fact indicates that even under perfect circumstances, CO emission is insensitive to a significant fraction of a cloud's total mass and that dust extinction measurements provide a more complete inventory of a cloud's total mass content.

Widefield extinction maps can also provide a relatively complete inventory of dense cores within cloud complexes. For example, 170 distinct cores were identified within the Pipe Nebula from an analysis of its extinction map (*Lombardi et al.,* 2006). The sizes and masses of this population of cores are readily obtained from the extinction data. Since dense cores are the progenitors of stars, the core mass function of a cloud is of particular interest for developing a theory of star formation. Figure 5 shows the core mass function (CMF) for the Pipe Nebula (Alves et al., in preparation) and the stellar IMF for the Trapezium cluster (*Muench et al.,* 2001) plotted for comparison. The shape of the Pipe CMF is surprisingly very similar to that of the stellar IMF. This similarity has potentially profound implications for star formation.

Although molecular-line studies (e.g., *Blitz,* 1993) have long suggested that the forms of the stellar and core mass functions were fundamentally different, observations of dust emission in a few regions hinted at a similarity of the shapes, at least for relatively high (>2–3 $M_\odot$) mass (e.g., *Motte et al.,* 1998; *Testi and Sargent,* 1998). Such a similarity would imply a 1-to-1 mapping of cores to stars in the star-formation process and indicate that the origin of the stellar IMF has its direct roots in the origin of the CMF. The extinction derived CMF of the Pipe Nebula is the first to reveal a break in the power-law form of the CMF at low mass (~2 $M_\odot$). This break is similar to that in the stellar IMF but occurs at a mass a factor of ~3 higher than the corresponding break in the stellar IMF (see Fig. 5). However, if the stellar IMF is shifted to higher mass by a multiplicative factor of about 3, the shapes of the two mass functions agree extremely well over all masses. The close correspondence in shape between the two mass functions indicates that there is indeed a direct transformation of the CMF to the stellar IMF. However, the factor of 3 difference in the mass scale is fundamentally significant since it further indicates that this transformation is governed by a universal efficiency of ~30% across the entire stellar mass range. The important implication of this observation is that understanding the origin of the stellar IMF requires understanding the origin of the mass spectrum of their progenitor cores. It is interesting that the Pipe CMF and the stellar IMF are so similar. The stellar IMF plotted is for stars formed in the Trapezium cluster where the environment and physical conditions differ significantly from those found in the Pipe Nebula, although the former are probably typical of those characterizing most star formation, since most stars are believed to be formed in clusters (*Lada and Lada,* 2003). This similarity may be another indication that the stellar IMF is a very robust product of the star-formation process.

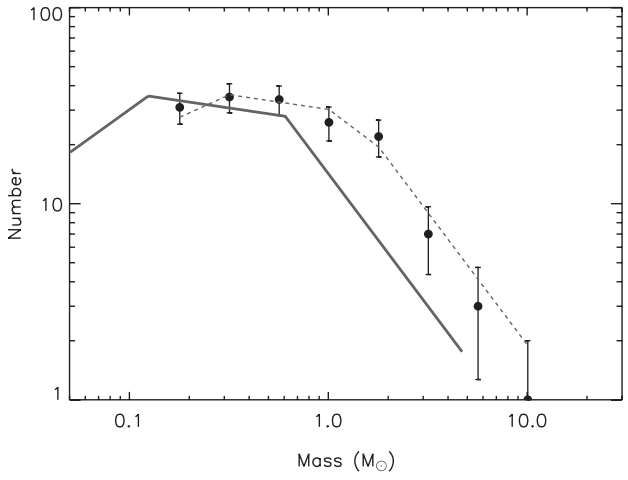

Fig. 5. The mass function of dense cores in the Pipe Nebula (Alves et al., in preparation). The points with error bars represent the observed core mass function. The solid trace on the left of the diagram is the stellar IMF derived for the Trapezium cluster (*Muench et al.,* 2002), which is very similar to the galactic field star IMF. The dotted trace passing through the points on the right is the stellar IMF scaled by a factor of 3 in mass and binned to the same mass intervals as the core mass function. The two mass functions have very similar shapes (apart from the factor of 3 shift in mass scale).

5. COMPARISON WITH MOLECULAR DATA

Infrared extinction measurements provide the most straightforward way to make direct determinations of molecular abundances in regions of high extinction (i.e, A_V > 5 mag). Such measurements are therefore critical to quantitative exploration of cloud chemistry and chemical evolution. In Fig. 6 we show the map of $C^{18}O$ emission of the B68 cloud along with a detailed point-to-point comparison of the CO integrated intensity with extinction across the entire cloud (*Bergin et al.,* 2002). The spatial map clearly shows the CO emission to peak in a ring around the cloud center. Comparison with the extinction map in Fig. 2 shows that CO and extinction are essentially anticorrelated in the sense that CO is apparently absent where the extinction is the highest.

The relation between integrated intensity and dust optical depth is linearly correlated (but with significant scatter) until a visual opacity of about 10 mag, at which point there is a sharp break followed by a flattening and then a decrease in the integrated intensity with increasing cloud extinction. Calculations of the non-LTE excitation of CO that directly incorporate the observed Bonnor-Ebert density distribution derived from the extinction indicate that the observed emission is largely optically thin. This, in turn, is confirmed by

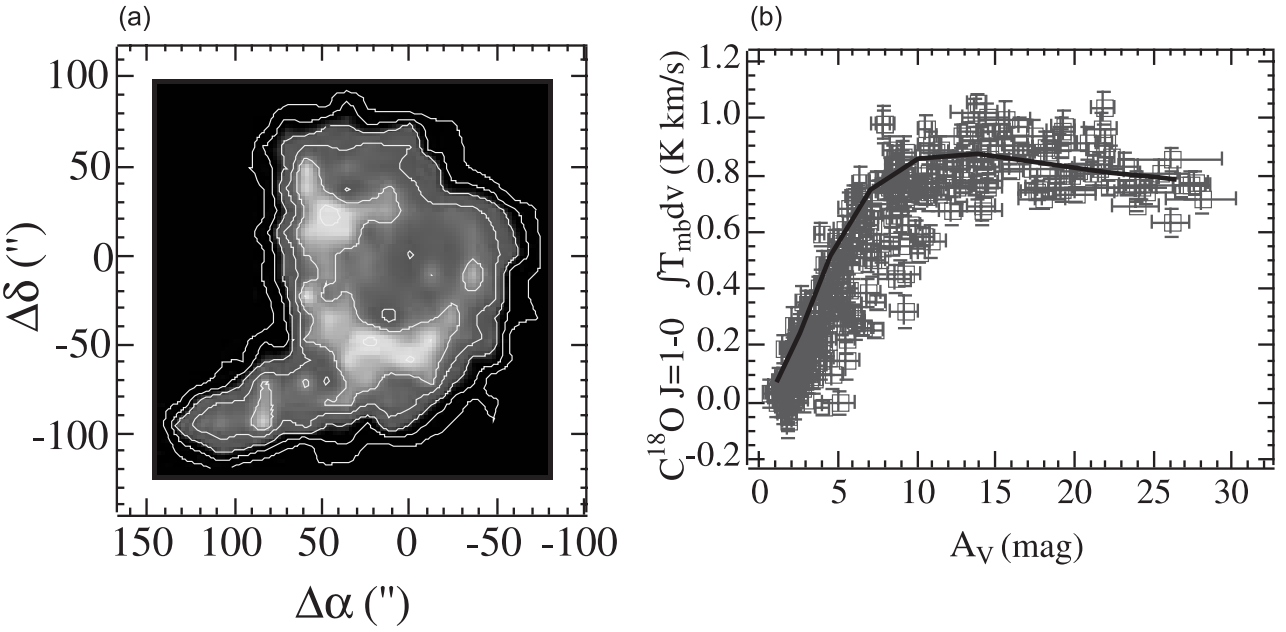

Fig. 6. **(a)** Map of $C^{18}O$ (J = 1–0) emission from the B68 cloud together with **(b)** a plot of the correlation between CO integrated intensity and extinction for the cloud. The break from a linear correlation at 10 mag in the latter plot indicates a sharp decrease of CO abundance in the high-extinction regions. This drop in abundance in the central regions is also manifest in the spatial map, where a bright ring of emission surrounds a central depression. The solid line in the righthand plot represents the prediction of a chemical model in which the CO abundance is decreased by 2 orders of magnitude in the central regions of the cloud due to depletion onto grains (from *Bergin et al.,* 2002).

observations of the rarer $C^{17}O$ isotope at numerous locations (*Bergin et al.,* 2002). Thus, the flattening of the relation is due to a sharp decline in the CO abundance in the center of the cloud. Indeed the inner regions may be completely devoid of gaseous CO. In a similar fashion Bergin et al. also measured the abundances of CS and N_2H^+ across the cloud and demonstrated a pattern of differential depletion for these species in which CS is most heavily depleted and N_2H^+ is least depleted of the species observed. This pattern of depletion agrees with predictions of models of time-dependent chemical evolution. This is illustrated by the chemical model plotted in Fig. 6, which matches the data very well and requires a reduction in the CO abundance of over 2 orders of magnitude. These observations and calculations suggest that in the very center of the cloud all observable molecules may be frozen onto grains, except perhaps for a species such as H_2D^+. Very similar results have been derived from extinction studies of other clouds (*Kramer et al.,* 1999; *Bergin et al.,* 2001) and from studies comparing molecular and dust emission from clouds (*Caselli et al.,* 1999; *Tafalla et al.,* 2002). Together these observations show that it may not be possible to probe the conditions in the inner regions of prestellar cores with molecular-line tracers and that maps of the distribution of dust are the most reliable tracers of cloudy material at the highest extinctions.

Combining infrared extinction data with molecular-line observations of the more abundant CO isotopes, particularly ^{12}CO and ^{13}CO, can provide important constraints for determining masses of GMCs in the Milky Way and in other galaxies where measurements of dust may be difficult or impractical. One of the standard methods to determine cloud masses of galactic and extragalactic GMCs is to scale CO integrated intensities by the so-called "X-factor," which is defined to be the ratio of total column density to CO integrated intensity. Direct comparisons of CO observations with infrared extinction measurements at thousands of points within a molecular cloud have greatly improved the determination of the X-factor (e.g., *Lada et al.,* 1994; *Lombardi et al.,* 2006). These studies find a definite linear correlation between CO integrated intensity and extinction over the range $2 < A_V < 6$ mag. Below an A_V of 2, CO is dissociated and undetectable, while above an A_V of 6, the CO lines are optically thick and the correlation saturates. However, both studies find a large intrinsic scatter in the correlated quantities. The correlation coefficient is low (~0.5) for both the observed ^{12}CO- (*Lombardi et al.,* 2006) and ^{13}CO-extinction correlations.

These CO-extinction comparisons indicate that there is an intrinsic and irreducible uncertainty of about a factor of ~1.4–2.0 in the X-factor. The likely reason for this circumstance is the volatile chemistry that must characterize the

low extinction regions of GMCs where most of the mass is found (*Lada et al.,* 1994).

6. EXTINCTION MAPPING OF GALAXIES

The physics of the formation of GMCs is one of the major unsolved problems of the interstellar medium. Although many papers have been written on the subject (for a review, see *Elmegreen,* 1993, and references therein) it is not yet known what the dominant formation mechanism is, nor even what the relative importance of gravity, shocks, and magnetic fields are in the cloud-formation process. One avenue for testing these theories is to study molecular clouds in a wide range of environments, ideally from a view point outside the galaxy's plane, and to determine which aspects of the environment set the cloud properties.

A study of GMCs in external galaxies can address the fundamental questions of whether the molecular ISM in external galaxies is organized differently than in the Milky Way and whether GMCs play the same central role in massive star formation as in the Milky Way, and are then responsible for galaxy evolution. Moreover, in an external galaxy we can easily disentangle molecular clouds and assess their basic properties and star forming status, as opposed to the confused "inside view" of GMCs. Ironically, GMCs are perhaps the most overlooked parameter in extragalactic star formation studies, and only recently, with the development of millimeter (CO) interferometry, they are beginning to be consistently incorporated into the picture.

In the previous sections we presented the merits of deep NIR imaging to trace column density not only in dense cores but also entire molecular cloud complexes where these dense cores are embedded (see Fig. 4). Recently, we have been trying to extend this successful idea to extragalactic GMCs. Instead of measuring the color of thousands of background stars to molecular clouds, we will measure the average color of the unresolved thousands of stars that will fall on a pixel of a NIR detector. We will measure the NIR diffuse galaxy light seen through GMCs, in a simple analogy to our galactic work. Dark dust lanes (as judged by available deep optical imaging), and a bright diffuse background, are necessary conditions to make the method work. It is easy to understand the impact this approach might have when one realizes that we will be able to map the distribution of dust column density at subarcsecond resolutions better than present-day interferometers (with typical resolutions of a few arcseconds; see Fig. 7). A caveat that does not affect our galactic work on the nearby complexes is the unknown contribution of foreground light along the line-of-sight. This contribution will dilute the signal, and without modeling, any derived column density along a specific line-of-sight will be a lower limit to the true column density. Still, one can minimize this problem by selecting targets with conspicuous dark lanes as seen in deep optical images.

Bialetsky et al. (in preparation) and Alves et al. (in preparation) present the first successful application of this extension of the technique to the radio-galaxy Centaurus A (NGC 5128) (Fig. 7). We have successfully mapped dust extinction in this galaxy down to a 3σ level of 0.7 mag (visual) and a physical resolution of 10 pc, i.e., the seeing in the final NIR image (0.6"). In our map we can resolve and identify individual GMCs. Figure 8 shows an optical (HST) image of a massive GMC associated with what appears to be an emerging or recently emerged OB association or young cluster. Next to the optical image is the derived infrared extinction map. This map of dust column density closely traces the optically obscured material that defines the cloud. We were able to identify more than 400 GMCs from our map of NGC 5128 and derived, for the first time, a GMC mass spectrum ($dN/dM \propto M^{-\alpha}$) that does not rely on CO

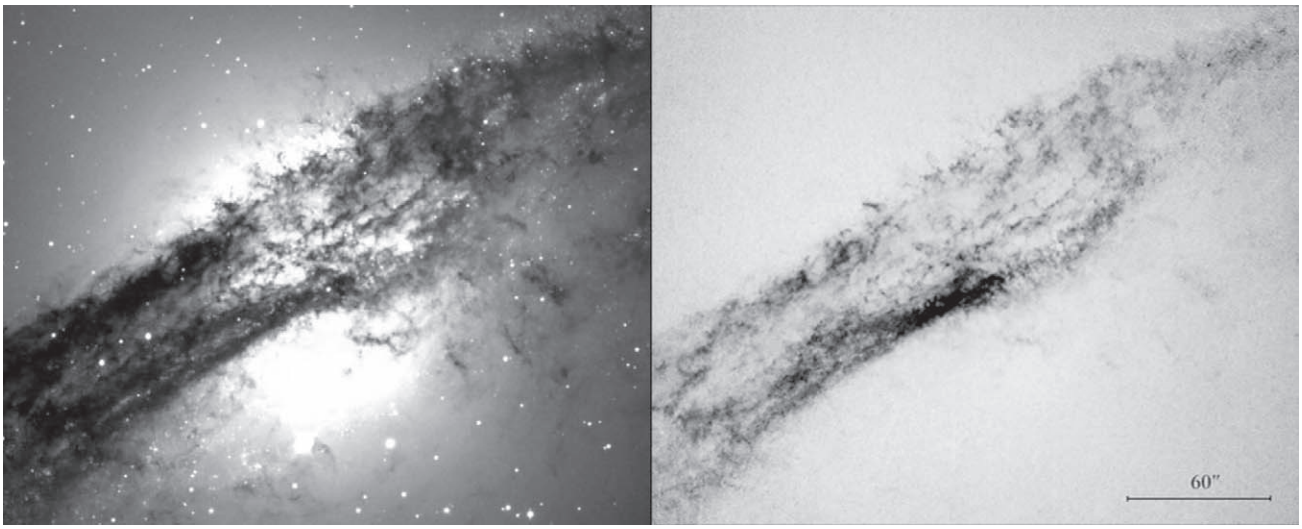

Fig. 7. Optical image and corresponding dust extinction map derived from near-infrared imaging of Cen A obtained with ESO's New Technology Telescope.

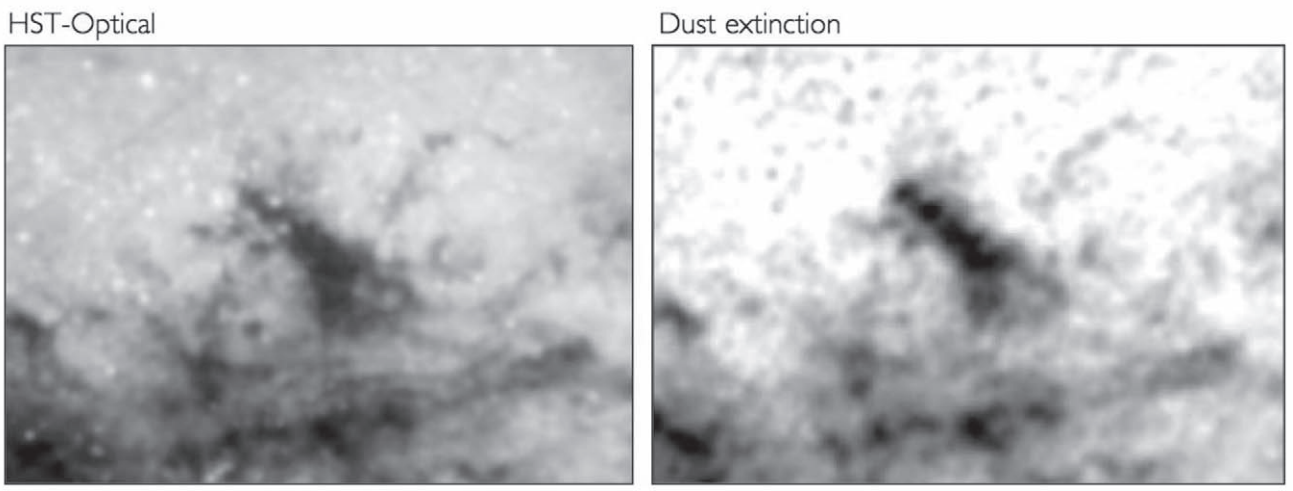

Fig. 8. Optical HST image and infrared extinction map zooming in on a single GMC with an associated, recently emerged young OB association/cluster within the Cen A dusty disk (see Fig. 7). The extinction map of dust column density clearly resolves the molecular cloud.

observations. The result, a Salpeter-like law ($\alpha \sim 2.31$), is puzzling as the CO-derived GMC mass spectrum for our galaxy and many others is $\alpha \sim 1.5$ (*Solomon et al.,* 1987; *Scoville et al.,* 1987). Overlap of GMCs along the line-of-sight could influence the mass spectrum that is derived for Centaurus A, but such an effect would lead to an apparent excess of more massive clouds and a flatter slope and smaller spectral index than derived. There is, nevertheless, a CO-derived GMC mass spectrum for M33 (*Engargiola et al.,* 2003) that is similar to our result, and we might be seeing an intrinsic and physical difference of GMCs in galaxies. There is also the possibility that because we are much more sensitive to column density, and have exquisite resolution when compared to CO data [the *Engargiola et al.* (2003) result uses an interferometer], we might be determining the true GMC mass spectrum in galaxies. This issue remains open and more observations of other galaxies are needed. Clearly, NIR dust column tracing in external galaxies is possible and promises to bring a new and complementary look to the morphology of the dense ISM in nearby galaxies.

7. CONCLUDING REMARKS

The development of infrared arrays has enabled the measurement and mapping of dust extinction in molecular clouds with unprecedented detail, depth, and precision. Such studies are providing new insights into the structure and structural evolution of dense cores. A clearer empirical and theoretical picture of core evolution from an initial state of quasistable equilibrium to the development of a protostellar embryo is now beginning to emerge. Mapping of large cloud complexes can produce very reliable estimates of total cloud mass and enable their structure to be quantified, facilitating comparison with theories of cloud evolution and star formation. Measurement of the core mass function is now possible for an interesting range of core mass and can be put on a reliable footing. Comparison with molecular-line observations yields improved determinations of molecular abundances and investigation of cloud chemistry. For example, such comparisons have produced some of the most compelling evidence for differential depletion in cold starless cores. Although not discussed here, comparison with observations of dust emission can produce important constraints on the nature of dust and on the thermal structure in cloud cores (*Kramer et al.,* 1998, 1999; *Bianchi et al.,* 2003). Finally, infrared extinction mapping techniques can be applied to investigate the star-forming clouds in external galaxies with angular resolution comparable to that of the best radio interferometers, including ALMA, and in doing so, provide an unexpected new window on the nature of extragalactic GMCs.

Acknowledgments. We thank the referee, R. Kandori, for a careful reading of this chapter and suggestions that improved its content. This work was partially supported by the NASA Origins Program under grants NAG 5-9520 and NAG 5-13041.

REFERENCES

Alves J. F., Lada C. J., Lada E. A., Kenyon S., and Phelps R. (1998) *Astrophys. J., 506,* 292–305.

Alves J. F., Lada C. J., and Lada E. A. (1999) *Astrophys. J., 515,* 265–274.

Alves J. F., Lada C. J., and Lada E. A. (2001a) *Nature, 409,* 159–161.

Alves J. F., Lada C. J., and Lada E. A. (2001b) *ESO Messenger, 103,* 1–20.

Ballesteros-Paredes J., Klessen R. S., and Vázquez-Semadeni E. (2003) *Astrophys. J., 592,* 188–202.

Barnard E. E. (1919) *Astrophys. J., 49,* 1–24.

Becklin E. E. and Neugebauer G. (1967) *Astrophys. J., 147,* 799–802.

Benson P. and Myers P. C. (1989) *Astrophys. J. Suppl., 71,* 89–108.

Bergin E. A., Ciardi D. R., Lada C. J., Alves J. F., and Lada E. A. (2001) *Astrophys. J., 557,* 209–225.

Bergin E. A., Alves J. F., Huard T. L., and Lada C. J. (2002) *Astrophys. J., 570,* L101–L104.
Bianchi S., Goncalves J., Albrecht M., et al. (2003) *Astron. Astrophys., 339,* L43–L46.
Blitz L. (1993) In *Protostars and Planets III* (E. H. Levy and J. I. Lunine, eds.), pp. 125–161. Univ. of Arizona, Tucson.
Bok B. J. (1948) In *Centennial Symposia,* pp. 53–72. Harvard College Observatory Monographs, Vol. 7, Cambridge.
Bok B. J. (1956) *Astron. J., 61,* 309–316.
Bok B. J., Lawrence R. S., and Menon T. K. (1955) *Publ. Astron. Soc. Pac., 67,* 108–112.
Bohlin R. C., Savage B. D., and Drake J. F. (1978) *Astrophys. J., 224,* 132–142.
Bonnor W. (1956) *Mon. Not. R. Astron. Soc., 116,* 351–359.
Casali M. M. (1986) *Mon. Not. R. Astron. Soc., 223,* 341–352.
Caselli P., Walmsley C. M., Tafalla M., Dore L., and Myers P. (1999) *Astrophys. J., 523,* L165–L169.
Cambresy L. (1999) *Astron. Astrophys., 345,* 965–976.
Cambresy L., Epchtein N., Copet E., de Batz B., Kimeswenger S., et al. (1997) *Astron. Astrophys., 324,* L5–L8.
Cambresy L., Beichman C. A., Jarrett T. H., and Cutri R. M. (2002) *Astron. J., 123,* 2559–2573.
Cernicharo J. and Bachiller R. (1984) *Astron. Astrophys. Suppl., 58,* 327–350.
Dickman R. (1978) *Astron. J., 83,* 363–372.
Dobashi K., Uehara H., Kandori R., Sakurai T., Kaiden M., Umemoto T., and Sato F. (2005) *Publ. Astr. Soc. Japan, 57,* 1–368.
Ebert R. (1955) *Z. Astrophys., 37,* 217–223.
Elmegreen B. G. (1993) *Astrophys. J., 419,* L29–33.
Engargiola G., Plambeck R. L., Rosolowsky E., and Blitz L. (2003) *Astrophys. J. Suppl., 149,* 343–363.
Harvey D. W., Wilner D. J., Lada C. J., Myers P. C., Alves J. F., and Chen H. (2001) *Astrophys. J., 563,* 903–918.
Harvey D. W., Wilner D. J., Lada C. J., Myers P. C., and Alves J. (2003) *Astrophys. J., 598,* 1112–1126.
Heiles C. (1969) *Astrophys. J., 156,* 493–499.
Herschel W. (1785) *Philos. Trans. LXXV,* 213–224.
Hotzel S., Harju J., and Juvela M. (2002) *Astron. Astrophys., 395,* L5–L8.
Johnstone D., Di Francesco J., and Kirk H. (2004) *Astrophys. J., 611,* L45–L49.
Jones T. J., Hyland A. R., Robinson G., Smith R., and Thomas J. (1980) *Astrophys. J., 242,* 132–140.
Kandori R., Nakajima M., Tamura K., Tatematsu K., et al. (2005) *Astron. J., 130,* 2166–2184.
Kirk J. M., Ward-Thompson D., and André P. (2005) *Mon. Not. R. Astron. Soc., 360,* 1506–1526.
Kramer C., Alves J., Lada C. J., Lada E. A., et al. (1998) *Astron. Astrophys., 329,* L33–L36.
Kramer C., Alves J., Lada C. J., Lada E. A., et al. (1999) *Astron. Astrophys., 342,* 257–270.
Lada C. J. and Lada E. A. (2003) *Ann. Rev. Astron. Astrophys., 41,* 57–115.
Lada C. J., Lada E. A., Clemens D. P., and Bally J. (1994) *Astrophys. J., 429,* 694–709.
Lada C. J., Alves J., and Lada E. A. (1999) *Astrophys. J., 521,* 250–259.
Lada C. J., Bergin E. A., Alves J. F., and Huard T. L. (2003) *Astrophys. J., 586,* 286–295.
Lada C. J., Huard T. L., Crews L. J., and Alves J. (2004) *Astrophys. J., 610,* 303–312.
Lada E. A. (1992) *Astrophys. J., 393,* L25–L28.
Lai S-P., Velusamy T., Langer W. D., and Kuiper T. B. H. (2003) *Astrophys. J., 126*, 311–318.
Lilley A. E. (1955) *Astrophys. J., 121,* 559–568.
Lombardi M. (2005) *Astron. Astrophys., 438,* 169–185.
Lombardi M. and Alves J. F. (2001) *Astron. Astrophys., 377,* 1023.
Lombardi M., Alves J. F., and Lada C. J. (2006) *Astron. Astrophys., 454,* 781–796.
McKee C. F. (1999) In *The Origin of Stars and Planetary Systems* (C. J. Lada and N. D. Kylafis, eds.), pp. 29–66. Kluwer, Dordrecht.
McKee C. F. and Holliman J. H. (1999) *Astrophys. J., 522,* 313–337.
Motte F., André P., and Neri R. (1998) *Astron. Astrophys., 336,* 150–172.
Mouschovias T. and Ciolek G. E. (1998) In *The Origins of Stars and Planetary Systems* (C. J. Lada and N. Kylafis, eds.), pp. 305–339. Kluwer, Dordrecht.
Muench A. A., Lada E. A., Lada C. J., and Alves J. F. (2002) *Astrophys. J., 573,* 366–393.
Myers P. C. (2005) *Astrophys. J., 623,* 280–290.
Nakano T. (1998) *Astrophys. J., 494,* 587–604.
Ostriker E., Stone J., and Gammie C. (2001) *Astrophys. J., 546,* 980–1005.
Pagani L., Bacmann A., Motte F., et al. (2004) *Astron. Astrophys., 417,* 605–613.
Predehl P. and Schmitt J. H. M. M. (1995) *Astron. Astrophys., 293,* 889–905.
Rieke G. and Lebosky M. (1985) *Astrophys. J., 288,* 618–621.
Ryter C., Cesarsky C. J., and Audouze J. (1975) *Astrophys. J., 198,* 103–109.
Scoville N. Z., Yun M. S., Sanders D. B., Clemens D. P., and Waller W. H. (1987) *Astrophys. J. Suppl., 63,* 821–915.
Solomon P. M., Rivolo A. R., Barrett J., and Yahil A. (1987) *Astrophys. J., 319,* 730–741.
Shu F. H., Adams F. C., and Lizano S. (1987) *Ann. Rev. Astron. Astrophys., 25,* 23–81.
Strom S. E., Strom K. M., and Grasdalen G. (1975) *Ann. Rev. Astron. Astrophys., 13,* 187–216.
Tafalla M., Myers P. C., Caselli P., Walmsley C. M., and Comito C. (2002) *Astrophys. J., 569,* 815–835.
Tafalla M., Myers P. C., Caselli P., and Walmsley C. M. (2004) *Astron. Astrophys., 416,* 191–212.
Teixeira P. S., Lada C. J., and Alves J. F. (2005) *Astrophys. J., 629,* 276–287.
Testi L. and Sargent A. I. (1998) *Astrophys. J., 508,* L91–L94.
Tomita Y., Saito T., and Ohtani H. (1979) *Publ. Astron. Soc. Japan, 31,* 407–416.
Yun J. L. and Clemens D. P. (1990) *Astrophys. J., 365,* L73–L76.
Wilking B. A., Lada C. J., and Young E. (1989) *Astrophys. J., 340,* 823–852.
Wilson R. W., Jefferts K. B., and Penzias A. A. (1970) *Astrophys. J., 161,* L43–L46.
Wolf M. (1923) *Astron. Nachr., 219,* 109–114.